Magnetic Resonance Imaging studies on neuropsychiatric systemic lupus erythematosus

Steens, S.C.A.

Reproducibility of brain ADC histograms

4

Reproducibility of brain ADC histograms

SCA Steens
F Admiraal-Behloul
JA Schaap
FGC Hoogenraad
CAM Wheeler-Kingshott
S le Cessie
PS Tofts
MA van Buchem

European Radiology 2004, 14 (3): 425-430

The aim of this study was to assess the effect of differences in acquisition technique on whole-brain apparent diffusion coefficient (ADC) histogram parameters, as well as to assess scan-rescan reproducibility. Diffusion-weighted imaging (DWI) was performed in 7 healthy subjects with b-values 0-800, 0-1000, and 0-1500 s/mm^2 and fluid-attenuated inversion recovery (FLAIR) DWI with b-values 0-1000 s/mm^2. All sequences were repeated with and without repositioning. The peak location, peak height, and mean ADC of the ADC histograms and mean ADC of a region of interest (ROI) in the white matter were compared using paired-sample *t*-tests. Scan-rescan reproducibility was assessed using paired-sample *t*-tests, and repeatability coefficients were reported. With increasing maximum b-values, ADC histograms shifted to lower values, with an increase in peak height ($p<0.01$). With FLAIR DWI, the ADC histogram shifted to lower values with a significantly higher, narrower peak ($p<0.01$), although the ROI mean ADC showed no significant differences. For scan-rescan reproducibility, no significant differences were observed. Different DWI pulse sequences give rise to different ADC histograms. With a given pulse sequence, however, ADC histogram analysis is a robust and reproducible technique. Using FLAIR DWI, the partial voluming effect of cerebrospinal fluid, and thus its confounding effect on histogram analyses, can be reduced.

Introduction

In many brain diseases, clinical reading of images generated by conventional magnetic resonance imaging (MRI) sequences provides adequate diagnostic information; however, there is increasing awareness of the added value of quantitative MRI techniques, including apparent diffusion coefficient (ADC) measurements from diffusion-weighted imaging (DWI)[1-5]. Diagnostically, the main application for DWI is in the early detection of ischemic stroke[2;6]. In this focal neurological disorder, therapeutic decision making may be assisted by determination of ischemic lesion sizes and the presence of an ischemic penumbra region on DWI and ADC maps[7;8].

Moreover, volumetric histogram analysis of ADC maps is emerging as a technique for quantitation of the extent of both visible and invisible parenchymal damage in the whole brain (global lesion load) in diffuse demyelinating and degenerative brain disorders[9-14]. For example, in a demyelinating disorder, such as multiple sclerosis, volumetric ADC histogram parameters of the global lesion load provide measures of structural brain damage and a potential tool for disease monitoring[15-17].

Recently, it has been demonstrated that variation in diffusion weighting and the application of cerebrospinal fluid (CSF) suppression using fluid-attenuated inversion recovery (FLAIR) DWI affects ADC values in regions of interest (ROIs)[18-26]. In this study, we assessed the effect of different maximum b-values (800, 1000, and 1500 s/mm^2) and the use of FLAIR on whole-brain ADC histogram parameters. In addition, we assessed reproducibility of ADC histograms that were based on different DWI sequences on our clinical scanner.

Materials and methods

Study design

Seven healthy volunteers (three women, four men; mean age 30 years, age range 25-37 years) with no history of neurological disease were scanned after written informed consent. In each volunteer DWI sequences with maximum diffusion weightings of 800, 1000, and 1500 s/mm^2 were performed to assess the influence of b-weighting on whole-brain ADC histograms. To assess the influence on an ADC histogram of adding a FLAIR prepulse to a DWI protocol, the sequence with maximum b-value of 1000 s/mm^2 was repeated with a FLAIR prepulse in each volunteer (FLAIR DWI). To assess the reproducibility of ADC histograms all sequences were repeated with and without repositioning in all subjects. Finally, to assess the potential influence of segmentation steps on whole-brain ADC histograms acquired with DWI and FLAIR DWI, mean ADC values of the whole segmented brain were compared with mean ADC values measured in ROIs in the white matter (WM).

MR imaging

Brain MRI was performed in the axial plane. Scans were aligned parallel to the plane through the anterior and posterior commissure and covered the whole brain. Scanning was performed on a Philips Gyroscan Intera ACS-NT 1.5-T MR scanner (Philips Medical Systems, Best, The Netherlands), equipped with hardware for echo-planar imaging (EPI) and shielded gradients. The

body-coil was transmitting, while the standard quadrature head-coil was in receiver mode. Multi-slice, single-shot DW-EPI of the whole brain was performed in three orthogonal directions (x, y, and z). For each diffusion direction a combination of x, y, and z gradients was used to apply strenghts of 30 mT/m and a slew rate of 150 mT/m s^{-1}. From the individual DWI images an isotropic diffusion image was calculated, from which an isotropic ADC map was derived. Additionally, an image with no diffusion weightings was acquired (b=0 s/mm^2). Geometric imaging parameters for all DWI sequences were as follows: field of view (FOV) 240 mm; scan matrix 128×128; and 44 contiguous slices of 3 mm thickness. To reduce scan time, a scan percentage of 60% was applied (resulting in an EPI factor of 77, 60% of 128). With this single-shot DW-EPI sequence, no cardiac triggering was applied and the repetition time was fixed per sequence. In the equation for diffusion weighting

$$b=\gamma^2G^2\delta^2\left(\Delta-\frac{\delta}{3}\right) \qquad \text{(equation 1)}$$

where γ is the gyromagnetic ratio, G is the gradient magnitude, δ is the diffusion time, and Δ the time between the onset of the diffusion gradients[2;27], δ and Δ were varied to achieve maximum diffusion weightings of 800, 1000, and 1500 s/mm^2, keeping G constant. For the sequences with b-values 0-800, 0-1000, and 0-1500 s/mm^2, respectively, δ was 20.1/22.1/26.1 ms, Δ 37.4/39.4/43.2 ms, echo time (TE) 74/74/84 ms, repetition time (TR) 6083/6694/7239 ms, number of signal averages (NSA) 1 for all, and scan times 43/47/51 s. Subsequently, a slice-selective inversion recovery (IR) pulse was added to the 0-1000 s/mm^2 sequence described previously, to suppress the signal of CSF at the moment of image acquisition (δ 22.1 ms, Δ 39.4 ms, TE 74 ms, TR 7350 ms, inversion time (TI) 2000 ms, NSA 2, scan time 103 s). A fat-saturation pulse was applied on all sequences to minimize chemical-shift artifacts. For postprocessing purposes, before repositioning the subject a three-dimensional T_1-weighted gradient echo sequence was performed with a FOV of 240 mm, scan matrix 256×256, TE/TR=12/29 ms, and 44 contiguous slices of 3 mm. Total scan time for all DWI sequences with rescanning and three-dimensional T_1-weighted scan was ±19 minutes.

Data processing and analysis

Magnetic resonance images of all subjects in this study were evaluated on both T_1- and b=0 s/mm^2 (T_2-) weighted images by a neuroradiologist and were all unremarkable. By calculating ADC from the isotropic diffusion map and the image without diffusion weighting for every voxel, ADC maps were created automatically online, and then transferred to an offline workstation for postprocessing (figure 1). Subsequently, ADC histogram parameters were generated fully automatically using an inhouse developed software package (SNIPER: Software for Neuro-Image Processing in Experimental Research). Image processing consisted of three main steps: (a) automatic brain stripping; (b) CSF segmentation; and (c) ADC histogram generation.

For automatic brain stripping (a), an average EPI image in a stereotaxic space (provided by the Montreal Neurological Institute) was first automatically registered to the b=0 s/mm^2 image using a 12-parameter affine transformation[28]. The standard deviation of ratio images was used

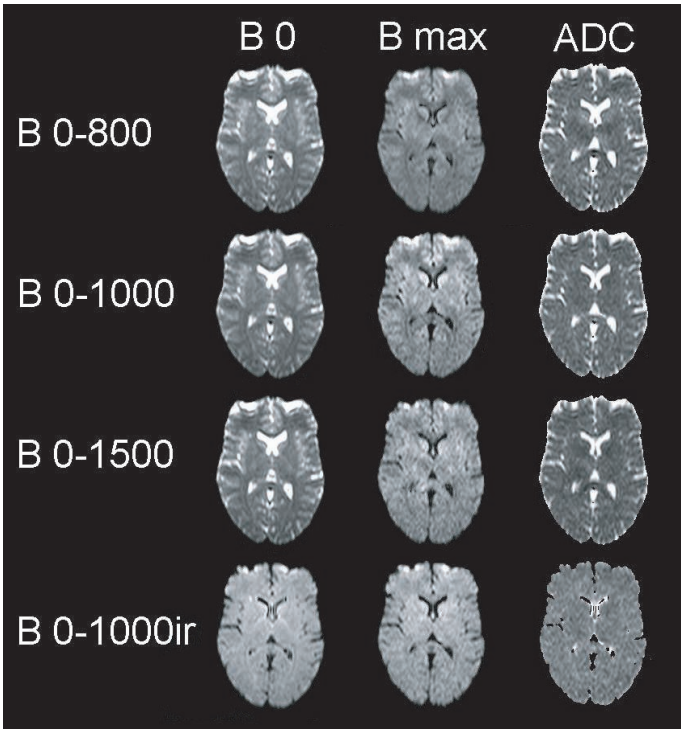

Figure 1. Diffusion-weighted images and apparent diffusion coefficient maps from diffusion-weighted imaging sequences with b-values 0-800 s/mm² (B 0-800), b-values 0-1000 s/mm² without fluid-attenuated inversion recovery (FLAIR; B 0-1000), b-values 0-1500 s/mm² (B 0-1500), and b-values 0-1000 s/mm² with FLAIR (B 0-1000ir).

as cost function. The resulting transformation matrix was then used to resize and reslice an intracranial prior probability map in order to mask automatically non-brain voxels (skin, bone, and eyeballs). For a more accurate intracranial delineation, a foreground vs background (two clusters) fuzzy clustering was performed. Mathematical morphology filters (opening and closing) were then applied to delete (or reduce as much as possible) the intracranial-skin connections. A region-growing algorithm, automatically seeded in the brain and constraint to remain within the resliced intracranial map, was finally applied. The ADC map was then automatically segmented into parenchyma and CSF (b) using fuzzy clustering (two clusters, parenchyma and CSF). Voxels belonging to the CSF cluster with a membership degree higher than 0.3 were classified as CSF. Voxels with CSF membership degree value between 0.3 and 0.6 are mainly partial volume. By assigning them to CSF the effect of partial volume on the histogram measurements was reduced. All segmentations (intracranial and brain parenchyma) were approved by an experienced observer. Finally, ADC histograms were generated (c) and normalized across the subjects for differences in brain size by division by the total number of voxels in the individual histograms. From these normalized histograms, several parameters were calculated: the location of the peak (10^{-6} mm^2/s), the peak height (10^{-3}, no unit), and mean ADC (10^{-6} mm^2/s). The whole data-processing procedure did not exceed 2 minutes (on average) per scan on a desktop computer.

Additionally, ROIs were drawn on the three-dimensional T_1-weighted images in the WM of the centrum semiovale in the left and right hemisphere, and subsequently copied to the ADC maps of the initial four DWI sequences. Because of potential differences in distortion with the three-dimensional T_1-weighted images, after placement on the three-dimensional T_1-weighted images all ROIs were visually inspected on the ADC maps. For the left and right hemisphere ROI, the mean ADC of both was calculated (volumes 1430±155 voxels or 3775±409 mm^3).

Statistical analysis

To evaluate the effect of changes in maximum b-value and the use of FLAIR, paired-sample *t*-tests were performed on the ADC histogram peak location, peak height, and mean ADC and ROI mean ADC for the sequences with maximum b-values 800 vs 1000 s/mm^2, 1000 vs 1500 s/mm^2, and 1000 s/mm^2 with FLAIR vs 1000 s/mm^2 without FLAIR. Analysis of scan-rescan reproducibility with and without repositioning was performed using paired-sample *t*-tests and repeatability coefficients[29]. All significance thresholds were set at 0.01.

Results

Changes in maximum b-value

A stepwise increase in the maximum b-value from 800 via 1000 to 1500 s/mm^2 resulted in a significant increase in the height of ADC histogram peaks (2.99-3.38-3.60×10^{-3}, respectively), with a significant shift of the peak to lower values (736-708-657×10^{-6} mm^2/s), and a significantly decreasing mean ADC (750-724-674×10^{-6} mm^2/s). Similarly, the mean ADC of the ROIs decreased significantly with increasing maximum b-values (751-708-642×10^{-6} mm^2/s).

DWI versus FLAIR DWI

Adding an IR prepulse to the DWI sequence with a maximum b-value of 1000 s/mm^2 (FLAIR DWI) resulted in ADC histograms with narrower, significantly higher peaks (3.74-3.38×10^{-3} for the DWI sequence with and without FLAIR), that were shifted to lower ADC values (peak location 690-708x10^{-6} mm^2/s conform, figure 2, trend towards significance, p=0.034). Furthermore, it resulted in significantly lower mean ADC values (699-724×10^{-6} mm^2/s, conform) and significantly higher volume estimates of the brain (446-379×10^3 voxels, conform). In the ROIs in the centrum semiovale, on the other hand, mean ADC values were similar using DWI sequences with and without FLAIR (701-708×10^{-6} mm^2/s, p=0.288; figure 3).

Scan-rescan reproducibility

With a given DWI sequence, scan-rescan reproducibility revealed no significant differences for all ADC histogram parameters with and without repositioning. The repeatability coefficients, which display the difference that will only be exceeded by 5% if the measurement is repeated on the same subjects, were calculated from the standard deviation of the mean differences[29]. For rescan without repositioning these were 0.17, 0.11, 0.12, and 0.15×10^{-3} for the peak height for sequences with b-values 0-800, 0-1000, and 0-1500 without FLAIR, and 0-1000 s/mm^2 with FLAIR, respectively, 1.5, 21.9, 31.0, and 24.3×10^{-6} mm^2/s for the peak location, and 14.4, 12.6, 11.8, and 10.9×10^{-6} mm^2/s for the mean ADC. Scanning with repositioning revealed repeatability

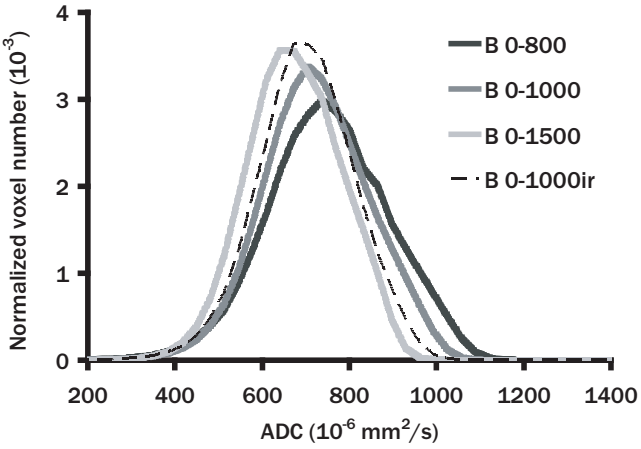

Figure 2. Average apparent diffusion coefficient (ADC) histograms of all subjects for sequences with b-values 0-800 s/mm² (B 0-800), b-values 0-1000 s/mm² without fluid-attenuated inversion recovery (FLAIR, B 0-1000), b-values 0-1500 s/mm² (B 0-1500), and b-values 0-1000 s/mm² with FLAIR (B 0-1000ir; normalized for volumes).

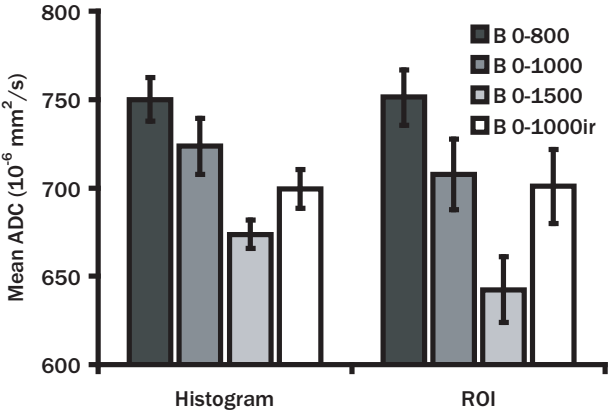

Figure 3. Mean apparent diffusion coefficient (ADC) values for the ADC histograms and regions of interest (ROI) for sequences with b-values of 0-800 s/mm² (B 0-800), 0-1000 s/mm² without fluid-attenuated inversion recovery (FLAIR, B 0-1000), b-values 0-1500 s/mm² (B 0-1500), and b-values 0-1000 s/mm² with FLAIR (B 0-1000ir) averaged over the seven volunteers. Visualized with error bars are the 95% confidence intervals. Mean ADC for the ROIs are the average values of the left and right hemisphere.

coefficients of 0.12, 0.17, 0.09, and 0.09×10^{-3} for the peak height for sequences with b-values 0-800, 0-1000, and 0-1500 without FLAIR, and 0-1000 s/mm² with FLAIR, respectively, 5.5, 22.0, 22.0, and 33.7×10^{-6} mm²/s for the peak location and 16.0, 21.7, 9.8, and 16.9×10^{-6} mm²/s for the mean ADC.

Discussion

In this study, we demonstrated that differences in DWI sequence parameters give rise to significant differences in volumetric ADC histograms; however, with a given DWI sequence, reproducible volumetric data can be obtained with repeated scanning.

A stepwise increase in the maximum b-value from 800 via 1000 to 1500 s/mm^2 resulted in an increasing height of the histogram peak, with a shift of the peak to the left, and a decreasing mean ADC for the brain. Similarly, increasing maximum b-values resulted in decreasing mean ADC values in ROIs in the WM. These observations can be explained by the work of Norris[30], who demonstrated that using sequences with high maximum b-values, signal is lost from the water component of tissues with high ADC values, a phenomenon that does not affect sequences with lower maximum b-values. The resulting filtering out of the high-ADC component of tissues with increasing maximum b-values gives rise to a decrease in the measured ADC values (the histogram shifts to the left). Since the remaining tissue is more homogeneous in terms of ADC values, the dynamic range of the histogram is also decreased. This phenomenon gives rise to narrowing and an increase in peak height, since the area under the curve of the ADC histogram remains equal.

The effect of adding an inversion recovery prepulse to a DWI sequence (FLAIR DWI) resulted in ADC histograms with narrower, higher peaks that were shifted to lower ADC values. Furthermore, it resulted in lower mean ADC values and higher volume estimates of the brain. These volumetric observations, which provide descriptives on the whole brain, contrast with observations in ROIs in the centrum semiovale. In these ROIs, mean ADC values were similar using DWI sequences with and without FLAIR, demonstrating that the observed differences in ADC histograms are not based on an effect of the prepulse on brain parenchyma per se[25;26]. The increase of brain volume and redistribution of pixels from the right tail of the histogram to the region of the peak in the FLAIR DWI suggest that, even after removal of CSF, partial volume effects at the brain-CSF interface still lead to inaccurately high ADC values in the sequence without FLAIR[10;22;25;26;31]. Additionally, the observation that ADC values measured in ROIs in the centrum semiovale, which only contained brain parenchyma and therefore did not suffer from partial voluming between brain parenchyma and CSF, were consistently lower than the observed mean ADC for the whole brain in the sequences without FLAIR, whereas they were much more similar in the FLAIR DWI sequence, supports this hypothesis.

Our observation that adding FLAIR to a DWI sequence provides ADC histograms that suffer less from partial volume effects at the brain-CSF interface is not trivial. Many degenerative brain diseases are associated with both atrophy and changes of the remaining brain parenchyma. Atrophy may give rise to widening of the sulci, and this may lead to an increased number of pixels at the brain-CSF interface that contain CSF and brain. Using a DWI sequence without FLAIR, this gives rise to an increased number of pixels with high ADC values. In general, degeneration of brain parenchyma also gives rise to increased diffusivity and therefore increased ADC values; thus, both processes may give rise to an increased number of voxels with increased ADC values, and the ADC histogram changes that are expected in such diseases may be attributed to atrophy as well as changes of the remaining brain tissue. Differentiating between these processes may be important but impossible. The ADC histograms based on FLAIR sequences do not suffer from that limitation, since an inclusion of CSF in a given voxel gives rise to a lower ADC value of that voxel as compared with voxels representing pure parenchyma, whereas disease-related increase of diffusivity gives rise to increased ADC values. Using FLAIR DWI, shifting of an ADC histogram to higher ADC values can thus only be attributed to increased diffusivity of brain tissue, and not

to atrophy. The FLAIR DWI sequences may thus provide better volumetric, quantitative estimates of the integrity of the (remaining) brain tissue than DWI sequences without FLAIR.

Repetition-time values for the non-FLAIR and FLAIR sequence with maximum b-value 1000 s/mm^2 were slightly different; however, this cannot explain our ADC histogram findings for two reasons. Firstly, in the FLAIR sequence the time for recovery of longitudinal magnetization after the inversion pulse was 5.4 s (TR~7.4 s, TI 2 s), in the non-FLAIR sequence time for recovery was 6.7 s. Normal WM has a T_1~0.7 s[32], and is thus fully relaxed for both TR values. Gray matter would be slightly more affected since T_1 is slightly longer, but still saturation would be small since TR is several times T_1. Secondly, ADC values are calculated by dividing signals collected at different b-values but same TR; therefore, T_1-saturation effects in a homogeneous voxel are divided out regardless of the specific TR value. If a voxel contains a mixture of protons in different (unconnected) pools having different T_1-values, the measured ADC is a weighted average of the values for each pool. As the weighting depends on the signal (and thus saturation) for each pool, it would be slightly dependent on TR; however, given the long TR and the scarcity of multi-exponential T_1-behavior, we believe this effect is negligible.

With a given DWI sequence, scan-rescan reproducibility showed no significant differences for all histogram parameters. In a heterogeneous population of patients with degenerative brain disorders, reproducibility as indicated by the repeatibility coefficients[29] is expected to be even higher than observed in this study, since the variation in ADC histogram parameters in such patients will be larger.

DWI sequences are sensitive to flow artifacts and motion from brain pulsations and gross head movements. In this study, a single-shot EPI sequence was used for DWI. Although single-shot EPI may suffer from magnetic field inhomogeneities causing image distortions and low spatial resolution, in a single excitation all information for reconstruction of one image is acquired[33]. Additionally, the short scan time and relative insensitivity to macroscopic motion (as opposed to multi-shot EPI sequences) improve image quality. Non-EPI sequences do not suffer from image distortions and low spatial resolution; however, these are often degraded by flow and motion artifacts because of longer scan times; therefore, EPI remains the method of choice for performing DWI[33].

Conclusion

The results of this study demonstrate that changes in DWI sequence parameters have a significant effect on ADC histograms; therefore, within one study, sequence parameters must be kept constant. With a given sequence, however, scan-rescan with and without repositioning returned good values. Furthermore, our results suggest that use of CSF suppression at the time of scanning reduces partial voluming effects, which limits the confounding effect of atrophy on whole-brain ADC histograms.

References

1. Gray L, MacFall J. Overview of diffusion imaging. Magn Reson Imaging Clin N Am 1998;6:125-138.
2. Schaefer PW, Grant PE, Gonzalez RG. Diffusion-weighted MR imaging of the brain. Radiology 2000;217:331-345.
3. Werring DJ, Brassat D, Droogan AG, Clark CA, Symms MR, Barker GJ, MacManus DG, Thompson AJ, Miller DH. The pathogenesis of lesions and normal-appearing white matter changes in multiple sclerosis: a serial diffusion MRI study. Brain 2000;123(Pt 8):1667-1676.
4. Naganawa S, Sato K, Katagiri T, Mimura T, Ishigaki T. Regional ADC values of the normal brain: differences due to age, gender, and laterality. Eur Radiol 2003;13:6-11.
5. Maldjian JA, Grossman RI. Future applications of DWI in MS. J Neurol Sci 2001;186 Suppl 1:S55-S57.
6. Roberts TP, Rowley HA. Diffusion weighted magnetic resonance imaging in stroke. Eur J Radiol 2003;45:185-194.
7. Lovblad KO, Baird AE, Schlaug G, Benfield A, Siewert B, Voetsch B, Connor A, Burzynski C, Edelman RR, Warach S. Ischemic lesion volumes in acute stroke by diffusion-weighted magnetic resonance imaging correlate with clinical outcome. Ann Neurol 1997;42:164-170.
8. El Koussy M, Lovblad KO, Kiefer C, Zeller O, Arnold M, Wels T, Buerki M, Oswald H, Schroth G. Apparent diffusion coefficient mapping of infarcted tissue and the ischaemic penumbra in acute stroke. Neuroradiology 2002;44:812-818.
9. Chun T, Filippi CG, Zimmerman RD, Ulug AM. Diffusion changes in the aging human brain. AJNR Am J Neuroradiol 2000;21:1078-1083.
10. Nusbaum AO, Tang CY, Buchsbaum MS, Wei TC, Atlas SW. Regional and global changes in cerebral diffusion with normal aging. AJNR Am J Neuroradiol 2001;22:136-142.
11. Huizinga TW, Steens SC, van Buchem MA. Imaging modalities in central nervous system systemic lupus erythematosus. Curr Opin Rheumatol 2001;13:383-388.
12. Bosma GP, Huizinga TW, Mooijaart SP, van Buchem MA. Abnormal brain diffusivity in patients with neuropsychiatric systemic lupus erythematosus. AJNR Am J Neuroradiol 2003;24:850-854.
13. Cercignani M, Iannucci G, Rocca MA, Comi G, Horsfield MA, Filippi M. Pathologic damage in MS assessed by diffusion-weighted and magnetization transfer MRI. Neurology 2000;54:1139-1144.
14. Filippi M, Inglese M. Overview of diffusion-weighted magnetic resonance studies in multiple sclerosis. J Neurol Sci 2001;186 Suppl 1:S37-S43.
15. Filippi M. In-vivo tissue characterization of multiple sclerosis and other white matter diseases using magnetic resonance based techniques. J Neurol 2001;248:1019-1029.
16. Wilson M, Morgan PS, Lin X, Turner BP, Blumhardt LD. Quantitative diffusion weighted magnetic resonance imaging, cerebral atrophy, and disability in multiple sclerosis. J Neurol Neurosurg Psychiatry 2001;70:318-322.
17. Bammer R, Fazekas F. Diffusion imaging in multiple sclerosis. Neuroimaging Clin N Am 2002;12:71-106.
18. Maier SE, Gudbjartsson H, Patz S, Hsu L, Lovblad KO, Edelman RR, Warach S, Jolesz FA. Line scan diffusion imaging: characterization in healthy subjects and stroke patients. AJR Am J Roentgenol 1998;171:85-93.
19. Sze G, Anderson A. Diffusing into the future. AJNR Am J Neuroradiol 2000;21:1780-1782.
20. Chen ZG, Li TQ, Hindmarsh T. Diffusion tensor trace mapping in normal adult brain using single-shot EPI technique: A methodological study of the aging brain. Acta Radiol 2001;42:447-458.

21. DeLano MC, Cooper TG, Siebert JE, Potchen MJ, Kuppusamy K. High-b-value diffusion-weighted MR imaging of adult brain: image contrast and apparent diffusion coefficient map features. AJNR Am J Neuroradiol 2000;21:1830-1836.

22. Clark CA, Le Bihan D. Water diffusion compartmentation and anisotropy at high b values in the human brain. Magn Reson Med 2000;44:852-859.

23. Melhem ER, Itoh R, Jones L, Barker PB. Diffusion tensor MR imaging of the brain: effect of diffusion weighting on trace and anisotropy measurements. AJNR Am J Neuroradiol 2000;21:1813-1820.

24. Burdette JH, Elster AD. Diffusion-weighted imaging of cerebral infarctions: are higher B values better? J Comput Assist Tomogr 2002;26:622-627.

25. Latour LL, Warach S. Cerebral spinal fluid contamination of the measurement of the apparent diffusion coefficient of water in acute stroke. Magn Reson Med 2002;48:478-486.

26. Falconer JC, Narayana PA. Cerebrospinal fluid-suppressed high-resolution diffusion imaging of human brain. Magn Reson Med 1997;37:119-123.

27. Cercignani M, Horsfield MA. The physical basis of diffusion-weighted MRI. J Neurol Sci 2001;186 Suppl 1:S11-S14.

28. Woods RP, Grafton ST, Holmes CJ, Cherry SR, Mazziotta JC. Automated image registration: I. General methods and intrasubject, intramodality validation. J Comput Assist Tomogr 1998;22:139-152.

29. Bland JM, Altman DG. Statistical methods for assessing agreement between two methods of clinical measurement. Lancet 1986;1:307-310.

30. Norris DG. The effects of microscopic tissue parameters on the diffusion weighted magnetic resonance imaging experiment. NMR Biomed 2001;14:77-93.

31. Kwong KK, McKinstry RC, Chien D, Crawley AP, Pearlman JD, Rosen BR. CSF-suppressed quantitative single-shot diffusion imaging. Magn Reson Med 1991;21:157-163.

32. Stevenson VL, Parker GJ, Barker GJ, Birnie K, Tofts PS, Miller DH, Thompson AJ. Variations in T1 and T2 relaxation times of normal appearing white matter and lesions in multiple sclerosis. J Neurol Sci 2000;178:81-87.

33. Nitz WR. Fast and ultrafast non-echo-planar MR imaging techniques. Eur Radiol 2002;12:2866-2882.